Supplemental Materials and Methods

Animals. All procedures, including animal experiments, were handled according to protocols approved by Swiss animal licenses VD2808/2808.1, VD2875/2875.1, VD3169 and VD3413 and according to the standard operating procedures of E-PHY-SCIENCE SAS (ENV/JM/MNO (2077)). Ten-week-old C57BL/6J male mice were purchased from Janvier Labs and allowed an acclimatization and handling period in the EPFL animal house for two weeks before experimentation. All animals were housed in groups of 4-5 animals at 22-25° C on a 12-hour light-dark cycle with food and water ad libitum.

Contextual fear conditioning (CFC). All behavioral testing was performed between 9AM and 1PM. The context groups in all experiments were exposed to the conditioning chamber for the same amount of time with no shocks. The chamber was cleaned with 5% ethanol between each animal.

Animal velocity (average cm/s) and distance travelled (total cm) during the habituation phases were calculated automatically by the TSE system. Changes in anxiety were determined by dividing the conditioning chamber int 36 sections and calculating the percent of total time each animal spent in the inner 16 section (no bordering wall) of the fear conditioning chamber during the initial habituation phase.

Rotarod. Motor performance was measured using a Rotarod apparatus (Bioseb, model LE8200). Mice were placed on the rotating rod, and the latency to fall was measured while the speed was accelerating from 4 to 40 rpm. Trials began when mice were placed on the rod and rotation began. Each trial ended, and latency was recorded, when the mouse fell off the rod. Mice were tested for 4 trials with a 1 minute inter-trial interval (1).

Electrophysiology. *Input/Output (I/O).* Synaptic transmission input/output (I/O) curves were constructed at the beginning of each experiment to asses basal synaptic transmission. For the I/O, a stimulus ranging from 0 to 100 µA by 10 µA steps was applied and measured every 5 secs.

Field excitatory postsynaptic potential (fEPSP). The following quality control and exclusion criteria were applied during the fEPSP analysis: A 10-min baseline-recording period preceded burst stimulation; signals with a fiber volley amplitude bigger than fEPSP amplitude and slices that failed to exhibit a linear increasing I/O curve were excluded from the analyses; likewise, slices that failed to show stable fEPSP slopes (> 15 % change) during this period and slices that not exhibiting a slope modification in either direction of at least 5 % after burst stimulation

were excluded from the analyses; slices that showed a decreasing slope reaching a close to null value were considered dying slices; potential outliers were identified for exclusion using mean ± 3x standard deviation.

Paired Pulse Facilitation (PPF). Paired Pulse Facilitation (PPF) was performed to assess short-term plasticity. For PPF, two stimulations were applied and measured at 50, 100, 150, 200, 300 and 400 ms intervals. PPF measurements were normalized by normalizing the first fEPSP slope to 1 and comparing it with the second fEPSP slope.

HDACi assay. Hippocampal and striatal hemispheres collected 1h after CFC were homogenized and incubated for 30-min on ice in RIPA buffer (150mM NaCl, 50mM Tris-HCl ph8, 0.1% SDS, 0.5% deoxycolate, 1% NP-40). Nuclear proteins were extracted in HDAC buffer (50mM Tris-HCl pH8, 137nM NaCl; 2.7mM KCl; 1mM MgCl2; 1mg/mL BSA) and sonicated for 15-min (Diagenode, Bioruptor Plus). Pan-HDAC enzyme activity was determined using the Fluor de Lys HDAC fluorometric activity assay kit (Enzo Life Science, BML-AK500). Fluorescence intensity (380nm excitation; 510 nm emission) was measured on a the Infinite M200 Pro (Tecan). Mice treated with VEH and not undergoing fear conditioning were considered as baseline HDAC activity.

RNA-seq. *RNA extraction and library preparation.* Single frozen hippocampal and striatal hemispheres from four biological replicates were isolated after CFC. Samples were homogenized and total RNA was isolated using Trizol Reagent (Life Technologies) according to the manufacturer's protocol. RNA was further purified by an on-column DNAse digestion using the RNase-Free DNase Set (Qiagen, Cat# 79254) and two rounds of washes using the RNAeasy Mini Kit (Qiagen, Cat# 74106). Total RNA concentration was determined with the Nanodrop 1000 (v3.8.1, Thermo Fisher).

Libraries were prepared using the TruSeq Stranded mRNA Preparation Kit (Illumina) starting from 900ng of RNA. Libraries were quantified with the dsDNA HS Assay kit (Qubit, Cat# Q32851) and profile analysis was performed using the TapeStation (Agilent, TS4200) D500 Screen Tape System (Agilent, Cat#5067- 5588 and 5067-5589). Finally, libraries were multiplexed and sequenced across five lanes on the Illumina HiSeq 4000 (Illumina), yielding 100-bp, paired-end reads, at EPFL's gene expression core facility.

RNA-seq analysis. Truseq adapter sequences were trimmed from raw FASTQ files using bcl2fastq (v2.20.0, Illumina). STAR (v2.6)(2) was used to align FASTQ reads to the mouse mm10 reference genome with annotations downloaded from Ensembl release 93(3). A custom R script was used to count reads mapping to the exonic regions of genes and to define

transcript abundance. Reads were only considered if they overlap a single gene region. Differential expression and downstream analysis were performed using DEseq2(4) and custom R scripts. Genes were considered differentially expressed if they had an adjusted p-value ≤ 0.05 and a $|\log_2 FC| \geq 0.4$. For the trajectory analysis, all experimental groups were compared to samples coming from VEH-Context animals (baseline). Genes were first grouped based on whether they were upregulated, downregulated or not changed between the VEH-CFC vs. VEH-Context. Next, each group was further divided based on whether they were more upregulated, more downregulated or not changed in the pair-wise comparison between HDACi-Context and VEH-Context. Finally, these subsets of genes were individually grouped based on their $\log_2 FC$ between the HDACi-CFC and the VEH-Context comparisons. Trajectory pathway analysis was performed using custom-written scripts in R.

Single-nuclear RNA-seq. *Library Preparation.* For single-nuclear RNA-sequencing (snRNA-seq) animals were treated with either VEH or HDACi and exposed to CFC. For each sample, both hippocampal hemispheres from 5 mice were pooled into two replicates each of VEH and HDACi treated groups. Nuclear extractions were performed as described. Nuclear structural quality was checked using an EVOS cell imaging system and nuclei were counted and diluted to 1,000 nuclei/μl.

Library Sequencing. Library constructions were performed using Chromium SingleCell 3'Reagent Kit v3 chemistry (10x Genomics) according to the manufacturers protocol (CG000183 - Rev A). All 4 libraries were pooled and sequenced across 2 NextSeq 500 (v2.5) chips for 75 cycles. FASTQ files were generated using cellranger mkfastq (CellRanger v3.0.1), yielding an R1 length of 28nt and an R2 length of 56 nucleotides.

snRNA-seq analysis. To generate single cell feature counts cellranger count (CellRanger v3.0.1) was run to align FASTQ files to the mm10 pre-mRNA genome (created using cellranger mkref (CellRanger v3.0.1)) using the following settings: expect-cells=4000, chemistry = SC3Pv3, r2-length = 56. These commands provide further information about the read lengths to expect after sequencing, the chemistry version used to create the 10x samples and the number of cells to expect based on what was recommended by the core facility (default is 3000). Downstream analysis was performed using custom R-scripts. Seurat (v4.0.3) (5) was used to calculate quality control metrics. DoubletFinder (6) was used to find and remove doublets and normalization and variance stabilization was done using SCTransform (7). Seurat was then used to perform UMAP and TSNE clustering, to define clusters using molecular identifiers. Differential expression analysis between VEH and HDACi treated groups was performed for each cell type using the logistic regression framework, accounting for

replicates, in Seurat's FindMarkers() command. Genes were considered differentially expressed if $|\log_2 FC| \geq 1$ and $P \leq 0.05$. This is in contrast to cutoffs used in the bulk RNA-sequencing as different tests were used as a logistic regression was used in Seurat's FindMarkers() and a negative binomial distribution was used in DESeq2 for the bulk RNA-sequencing. In addition, single nuclear compares UMI counts across hundreds of nuclei whereas bulk RNA-sequencing compares read counts across 4 replicates. Since this is cell-type specific, there are also differences in total expressed numbers of genes in each cell type compared to the bulk RNA-sequencing. These differences yield variable log2FC variation and it is best to be more stringent in the snRNA-sequencing analysis in order to get comparable proportions of DEGs in each analysis.

To determine what was causing the HDACi-mediated split seen in the UMAP for Excitatory Neurons of the DG and glial cell types, we performed an analysis in which we removed subsets of genes and re-clustered nuclei. Up ($\log_2 FC \geq 1$; $P \leq 0.05$) and downregulated ($\log_2 FC \leq -1$; $P \leq 0.05$) genes from the HDACi-Veh comparisons for each cell type were independently removed from the matrix of alignment counts. UMAP dimension reduction was then rerun on the subsetted counts to see whether those gene subsets were driving the cell type splits. This DEG removal test was performed using a custom written script in R.

Augur (8, 9) was used with default commands to calculate perturbation prioritization for each cell type and scProportionsTest (10) to compute cell type composition changes between HDACi and VEH treated samples.

Western Blots. Animals underwent HDACi administration and subthreshold CFC as described above. Full hippocampi were dissected and flash frozen 1 h after CFC. Frozen hippocampal hemispheres were cut in half, homogenized and incubated for 30 min on ice in 500μl RIPA buffer (150mM NaCl, 50mM Tris-HCl ph8, 0.1% SDS, 0.5% deoxycolate, 1% NP-40) with 20μl 20x protease inhibitor (Complete mini, EDTA-free, Sigma Aldrich Cat#11836170001). Nuclei were collected by centrifugation (max speed, 20 min, 4˚C) and cytoplasm (supernatant) was transferred to a new tube. The nuclear pellet was mixed with 50μl 1x Laemmli buffer, sonicated for 10 min at full power and boiled for 10 min at 90˚C or until samples were no longer viscous. Protein quantifications were performed using a DC assay. For each sample, 10μg protein was added to SDS-PAGE gel (12.5% acrylamide in Resolving Gel and 4.5% in stacking gel) and run at 25A for ~1.5 h. Proteins were then transferred to nitrocellulose membrane for 2 h at 4˚C and blocked for 1 h in 5% milk in PBS-Tween20. Primary antibodies (1:2500 H4K12ac (ab46983), 1:500 H3K9ac (ab10812), and

1:5000 H3K27ac (ab4729) in 2% milk + PBS-Tween20) were incubated with the membrane overnight at 4˚C (except 1:5000 total H3 (ab1791), incubated for only 30 min at RT). Then membranes were washed 3x in TBS-Tween20 and secondary antibodies (1:10,000 Goat anti-rabbit in 2% milk) for 1 h at RT. Membranes were washed and incubated with chemiluminescent ECL Plus (GE Healthcare, Cat# RPN2232SK) for 5 min before visualization on the Fusion FX Vilber Laurmat imaging system. Due to similar sizes of histone markers, blotting was done separately and stripped between each antibody.

To quantify chemiluminescence, images were analyzed using “Set Measurements” in ImageJ. For each blot, percent of total luminescence was calculated for each band and normalized to the respective H3 total luminescence. Technical replicates (same samples, 2 western blots) were averaged together for each antibody and per biological replicate (6 replicates per treatment).

ChIP-seq. *Nuclear sorting.* ChIP-seq was performed on 3 replicates per treatment and each replicate consisted of the pooled dentate gyri from 5 mice. After nuclear extraction (see above), filtered nuclei were cross-linked by incubating with 1% formaldehyde (AppliChem, A08770) for 5 min at RT. Cross-linking was quenched with 125mM glycine (VWR, 101196X) and nuclear structural quality was assessed using an EVOS FL cell imaging system (Life Technologies).

For each sample, approximately 750,000 nuclei were resuspended in 500μl PBS-T (PBS, 0.1% Tween 20). Nuclei were stained with 1:50 Alexa Fluor488 conjugated anti-NeuN antibody (Millipore, MAB377X) for 30 min, spun down (1250rcf, 4˚C, 5 min), washed in PBS-T (0.1% Tween 20) twice, resuspended and stored in 200μl PBS-T until sorting.

Flow cytometry was performed on the FACSAriaIII (BD Bioscience) by the EPFL Flow Cytometry Core Facility (FCCF). Before sorting, samples were passed through a 26G needle 5 times. Hoechst (1:1000) was mixed into each sample and incubated on ice for 10 mins. Debris was first excluded by gating using forward and side scatter pulse area parameters (FSC-A and SSC-A). Multiplets were then excluded by gating FSC-H vs. FSC-W and SSC-H vs. SSC-W. Single nuclei were sorted by Hoechst intensity, elicited by 405 nm wavelength excitation and measured at 425-475nm (450/50-A). Finally, NeuN+ nuclei were sorted into ice-cold Eppendorf tubes containing 100μl PBS-T.

Chromatin immunoprecipitation (ChIP). After sorting, nuclei were pelleted by centrifugation (4˚C, 1250g, 5 min) and lysed by incubating in 750μl RIPA buffer on ice for 10 min. Samples were sonicated on an E220 Focused-ultra-sonicator (Covaris) for 20 min (Peak power = 140W,

Duty = 5, Cycle/Burst = 200). Sonication efficiency was measured by decrosslinking 125µl of chromatin in 500µl of TL-Brain Buffer (10mM Tris-HCl pH7.5, 10mM EDTA 200mM NaCl), 50µl of 10% SDS and 1µl of RNAseA (Thermo Fisher, Cat#EN0531) and incubating at 65˚C and 650rpm overnight. 10µl recombinant, PCR-grade Proteinase K (Roche, Cat#03115828001) was added and incubated at 45˚C and 650 rpm for another hour. DNA was extracted with AcNH4 (100µl of 10M), 20µl glycogen (10µg/µl) and 1ml cold isopropanol and then pelleted by centrifuging at 14000rfc, 4˚C for 20 min. DNA was further purified in 1ml 70% EtOH and centrifuged (14000rfc, 4˚C, 10 min). Sonicated DNA size was assessed on a 1.5% agarose gel.

The rest of the ChIP experiment (beginning from "Protein G Agarose Bead Preparation") was carried out using the reagents and protocols from the Low Cell ChIP-Seq Kit (Active Motif, 53084). In brief, 400µl of sonicated chromatin was first cleared by incubating with pre-cleared Protein G agarose beads for 2 h on a rotator at 4˚C. Half was kept as input for each sample. The other half was immmunoprecipitated overnight at 4˚C with 3µl of H3K27ac (Abcam, ab4729). After precipitation, pre-cleared Protein G agarose were added for 3 h, and both input and IP samples were washed following the kit specifications. Cross-linking was reversed by incubating samples with 5µl 5M NaCl and 2µl proteinase K at 65˚C, 300rpm overnight. DNA was purified using phenol-chloroform.

Library preparation. To prepare libraries for both input and IP samples, the Next Gen DNA Library Kit (Active Motif, Cat# 53216) and Next Gen Indexing Kit (Active Motif, Cat# 53264) were used according to the manufacturer's instructions. After adaptor ligation, fragments were amplified (1 cycle, 30s at 98˚C; 14 cycles, 10s at 98˚C, 30s at 60˚C and 60s at 68˚C) and DNA was cleaned and purified using magnetic SPRI beads (Beckman Coulter, Ca# B23317). Libraries were resuspended in 25µl Low EDTA TE buffer and concentration was measured using a Qubit dsDNA HS Assay Kit. DNA fragments size was determined using a Fragment analyzer (NGS High Sensitivity kit (DNF-474), Agilent). Libraries were sequenced, paired-end, on the Illumina NextSeq 500 at EPFL's gene expression core facility**.**

ChIP-seq analysis. The Next Gen DNA Library Kit (Active Motif) includes molecular identifiers (MIDs), a 9-base random N sequence that is added with the P5 adaptor, to allow for removal of PCR duplicates from sequencing data. While R1 (75bp) contains the sequence information, R2 (9 bp) contains the MID information. To conserve MID information during mapping, the MID sequence from R2 was appended to the FASTQ header in R1 using a custom R-script. Adapter sequences and low quality regions from R1 were removed using Trimmomatic

(v0.38)(11) in single end mode with the following parameters: ILLUMINACLIP:Y2_adapter_seq.fa:0:6:6 SLIDINGWINDOW:10:20 MINLEN:36.

The processed FASTQ file (R1) was then aligned to the mm10 genome using Bowtie2 (v2.3.5)(12) in single-end mode and using default parameters. SAMtools (v1.9) (13) was used to convert SAM files to BAM format and then to sort BAM files. PCR duplicated alignments were removed from the BAM files using a perl script by Active Motif. Finally, multi-mapping and low-quality reads (≥ 40) were removed and BAM files were re-indexed using SAMtools.

Open chromatin peaks were defined using MACS2(14) in broad peak mode. Differentially acetylated regions (DARs) were identified using Diffbind (v2.16.2) (15) and DEseq2(v 1.28.1)(4) with default parameters. Peaks were considered differentially enriched if they had a false discover rate (FDR) ≤ 0.05 and $\left|\log_2\text{FoldChange}\right| \geq 1$.

Since H3K27ac is a marker for both promoters and enhancers, ChromHMM (v1.22)(16) was used to establish a chromatin state model that identified enhancers and promoters. The program was run, allowing for 8 states, on independently published ChIP-sequencing data (17), taken from bulk hippocampal tissue 1 h after CFC. The entire mouse genome was assigned to one of five chromatin states: Control regions; repressed regions; promoter regions; primed enhancers; and active enhancers (**Supplemental Fig. 14A**). We calculated the state overlap for each peak and assigned the peak to the state that covered the highest proportion (**Supplemental Fig. 14B**). Doing so, 70.5% of bases assigned as active enhancers in ChromHMM were enriched for H3K27ac in our dataset; 44% and 34.9% of bases assigned as primed enhancers and promoters, respectively, while only 2.8% and 2.9% of control regions and repressed regions had H3K27ac peaks (**Supplemental Fig. 14C**). This information was aligned with our own peak information to define differentially expressed enhancers and promoters. We assigned enhancers to genes using HOMER (v4.11) annotatePeaks.pl (18). Downstream trajectory analysis was performed (as described in the *RNA-sequencing Analysis* section) separately for peaks in different chromatins states.

All in-house analysis code can be found at https://github.com/allie-burns/2022_Burns_etal.

Supplemental References

1. M. A. Kheirbek, *et al.*, Adenylyl cyclase type 5 contributes to corticostriatal plasticity and striatum-dependent learning. *J. Neurosci.* **29**, 12115–12124 (2009).

2. A. Dobin, *et al.*, STAR: Ultrafast universal RNA-seq aligner. *Bioinformatics* **29**, 15–21 (2013).

3. D. R. Zerbino, *et al.*, Ensembl 2018. *Nucleic Acids Res.* **46**, D754–D761 (2018).

4. M. I. Love, W. Huber, S. Anders, Moderated estimation of fold change and dispersion for RNA-seq data with DESeq2. *Genome Biol.* **15**, 1–21 (2014).

5. Y. Hao, *et al.*, Integrated analysis of multimodal single-cell data. *Cell* **184**, 3573–3587 (2021).

6. C. S. McGinnis, L. M. Murrow, Z. J. Gartner, DoubletFinder: Doublet Detection in Single-Cell RNA Sequencing Data Using Artificial Nearest Neighbors. *Cell Syst.* **8**, 329–337 (2019).

7. C. Hafemeister, R. Satija, Normalization and variance stabilization of single-cell RNA-seq data using regularized negative binomial regression. *Genome Biol.* **20**, 296 (2019).

8. J. W. Squair, M. A. Skinnider, M. Gautier, L. J. Foster, G. Courtine, Prioritization of cell types responsive to biological perturbations in single-cell data with Augur. *Nat. Protoc.*, 1–42 (2021).

9. M. A. Skinnider, *et al.*, Cell type prioritization in single-cell data. *Nat. Biotechnol.* **39**, 30–34 (2021).

10. S. A. Miller, B. Policastro, scProportionTest (2020).

11. A. M. Bolger, M. Lohse, B. Usadel, Trimmomatic: A flexible trimmer for Illumina sequence data. *Bioinformatics* **30**, 2114–2120 (2014).

12. B. Langmead, S. L. Salzberg, Fast gapped-read alignment with Bowtie 2. *Nat. Methods* **9**, 357–359 (2012).

13. H. Li, *et al.*, The Sequence Alignment/Map format and SAMtools. *Bioinformatics* **25**, 2078–2079 (2009).

14. Y. Zhang, *et al.*, Model-based Analysis of ChIP-Seq (MACS). *Genome Biol.* **9**, R137 (2008).

15. R. Stark, G. Brown, DiffBind: differential binding analysis of ChIP-Seq peak data (2011).

16. J. Ernst, M. Kellis, ChromHMM: Automating chromatin-state discovery and characterization. *Nat. Methods* **9**, 215–216 (2012).

17. R. Halder, *et al.*, DNA methylation changes in plasticity genes accompany the formation and maintenance of memory. *Nat. Neurosci.* **19**, 102–110 (2016).

18. S. Heinz, *et al.*, Simple Combinations of Lineage-Determining Transcription Factors Prime cis-Regulatory Elements Required for Macrophage and B Cell Identities. *Mol. Cell* **38**, 576–589 (2010).

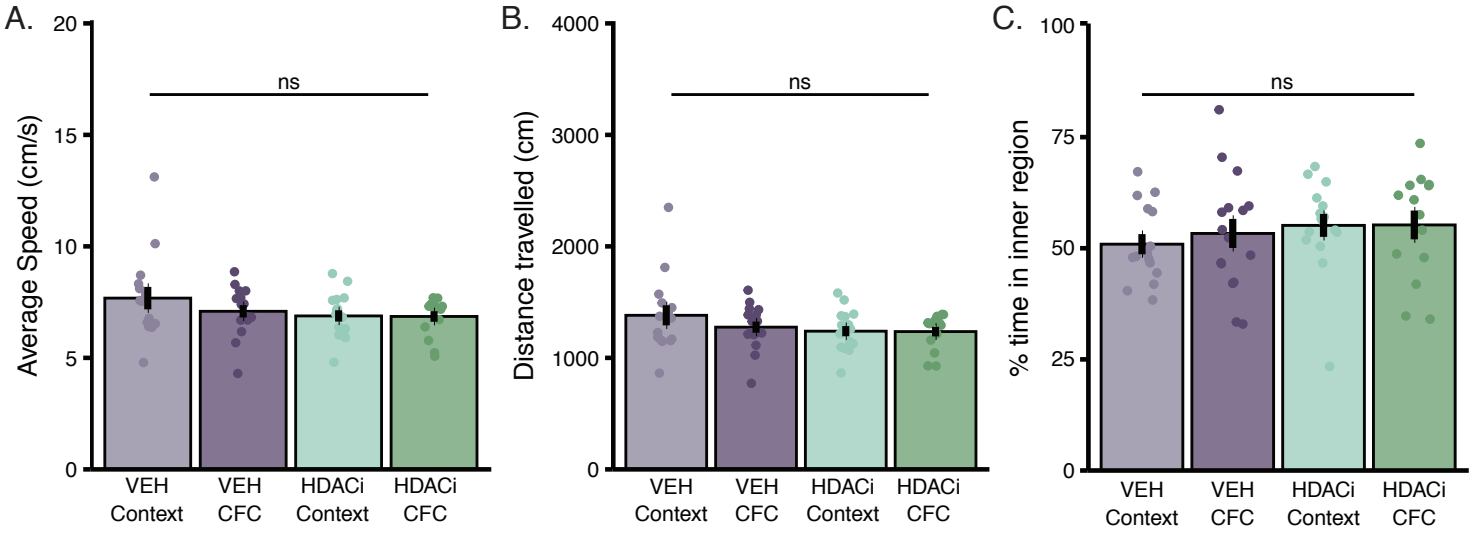

Supplemental Fig. 1. HDACi treatment does not affect speed, distance travelled or anxiety levels. (A) Average animal speed (cm/s) during the 3-minute habituation of behavioral conditioning was not affected by CI-994 injection. **(B)** Average distance travelled (cm) during the 3-minute habituation of conditioning was not different between Vehicle and CI-994 (HDACi) injection. **(C)** Time spent in inner regions of the conditioning chamber during the 3-minute habituation of conditioning did not change between Vehicle or CI-994 injection. One or two-way ANOVA with Tukey's HSD multiple comparisons test was used for analysis. Graphs represent mean ±SEM. ns = not significant. n (VEH-Context) = 15; n (VEH-CFC and HDACi-Context) = 16; n (HDACi-CFC) = 14.

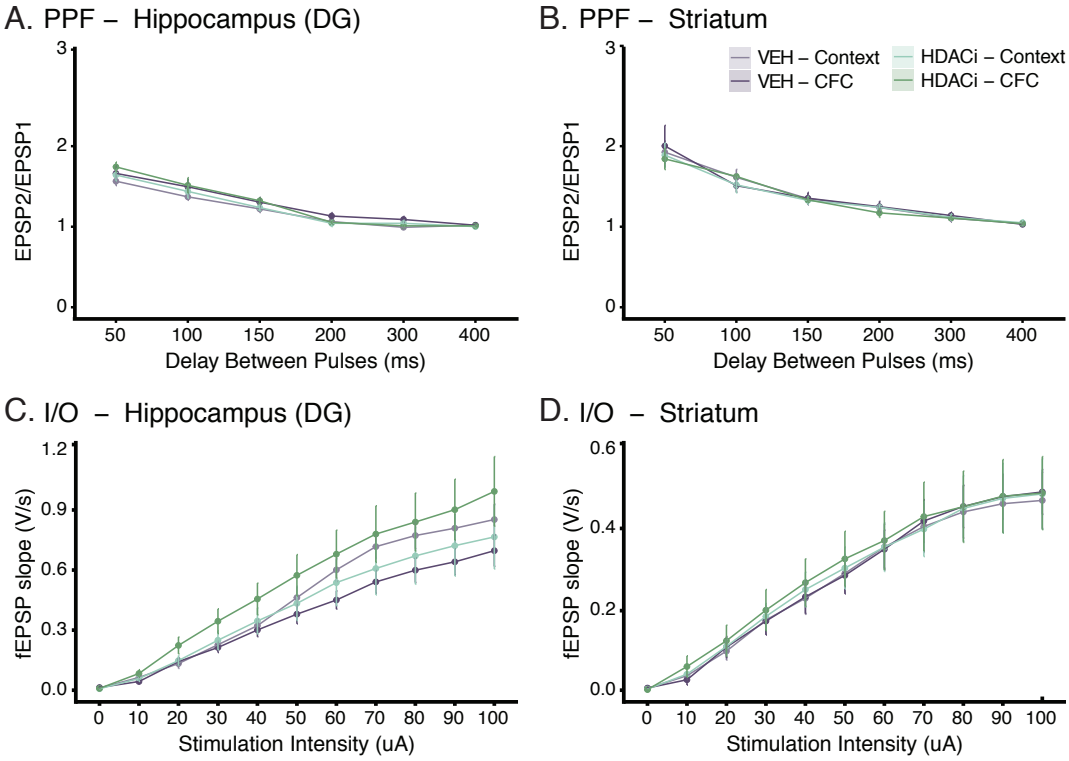

Supplemental Fig. 2. HDACi does not alter PPF or I/O in the hippocampus or striatum after CFC. (A and B) Paired pulse facilitation (PPF) in the DG **(A)** and striatum **(B)** 1 hour after CFC. **(C and D)** Input/output (I/O) relationship in the DG **(C)** and striatum **(D)** 1 hour after CFC. Graphs represent mean ±SEM. n = 8 animals/group.

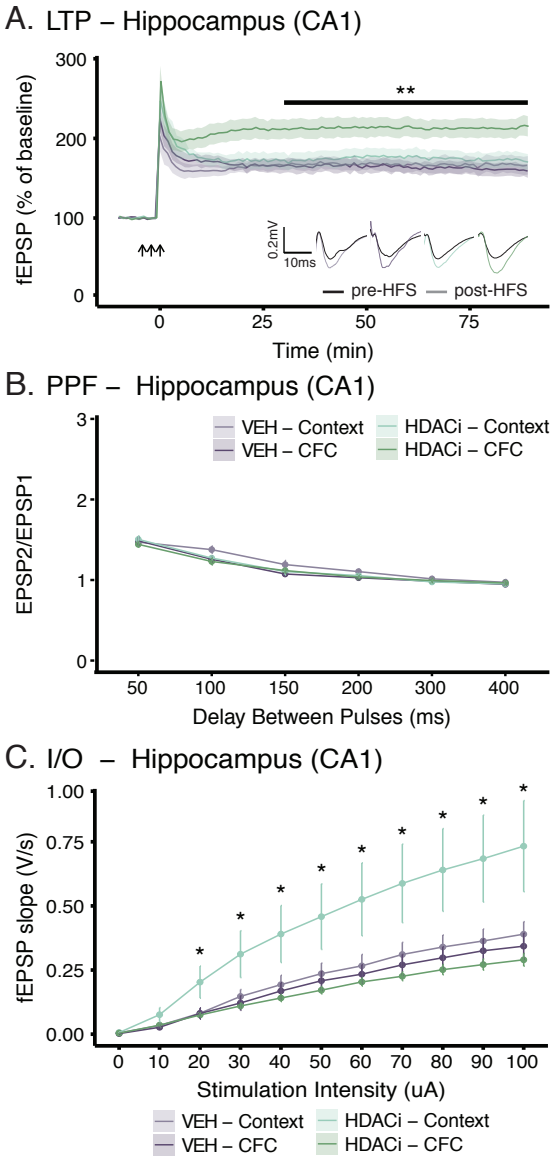

Supplemental Fig. 3. HDACi combined with CFC enhances LTP in hippocampal area CA1. (A) HDACi combined with CFC enhanced LTP in response to 3 trains of high frequency stimulation (HFS – arrows) at Schaffer Collaterals of the hippocampal CA1 one hour after behavioral training. Statistical differences were calculated for the 30 minutes (end of short-term-potentiation) to 90 minutes (end of recording) for each mouse. **(B)** There were no treatment-induced differences in PPF in the CA1. **(C)** HDACi-Context animals had a larger I/O relationship than other groups. Graphs represent mean ±SEM. * $P < 0.05$, ** $P < 0.01$. n = 8 animals/group.

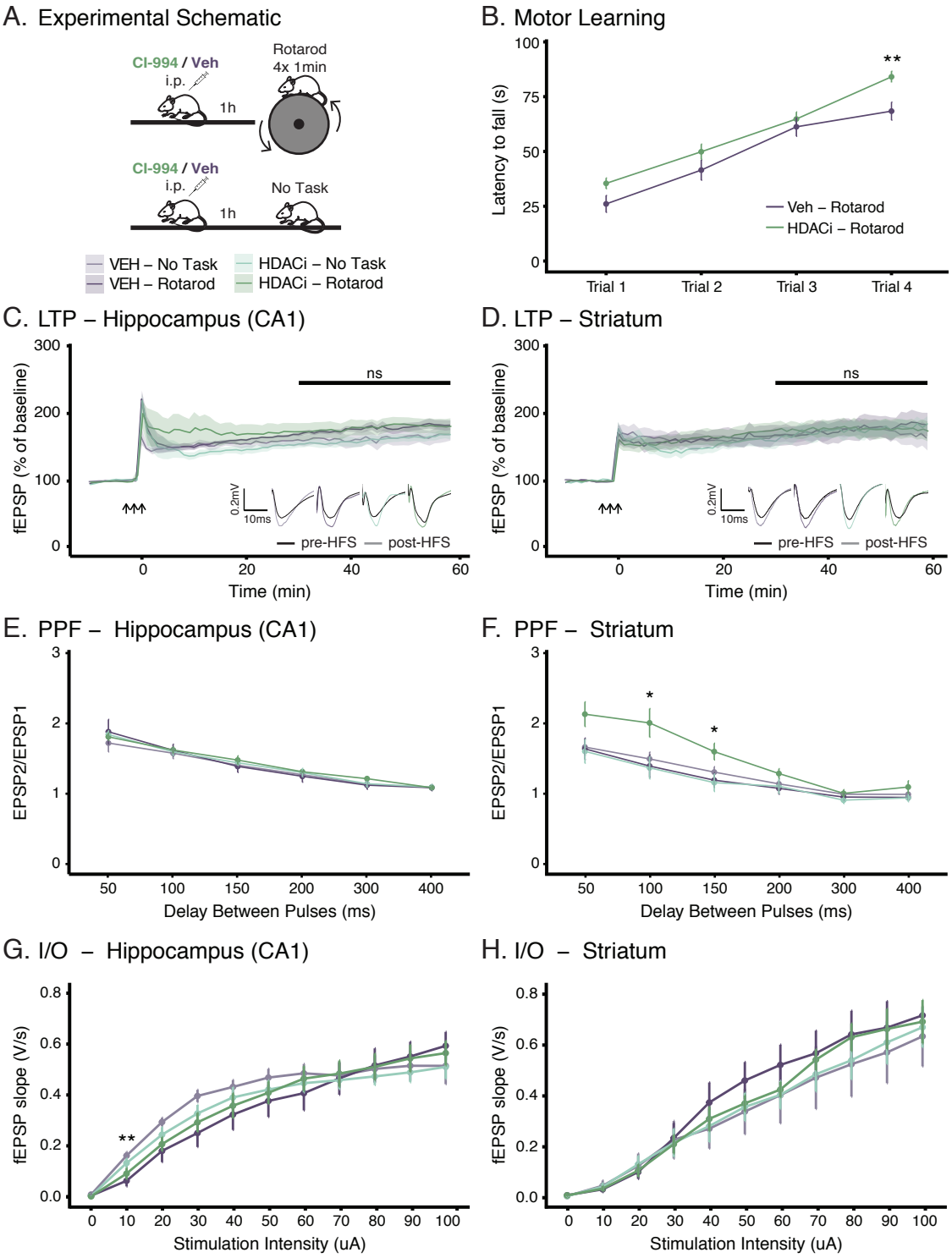

Supplemental Fig. 4. HDACi enhances PPF in the cortico-striatal pathway after motor learning. (A) Experimental schematic. Animals were i.p. injected with either Vehicle or CI-994 (30mg/kg) one hour prior to rotarod training. **(B)** HDACi combined with rotarod training increased the time to fall off the rotarod. **(C and D)** HDACi combined with rotarod training did not alter LTP in response to 3 trains of high frequency stimulation (HFS – arrows) in the Schaffer Collaterals of hippocampal CA1 **(C)** or in the cortical-striatal pathway **(D)** one hour after final rotarod trials. Statistical differences were calculated for the 30 minutes (end of short-term-potentiation) to 90 minutes (end of recording) for each mouse. **(E and F)** HDACi paired with rotarod training did not lead to any differences in PPF in the Schaffer Collaterals of the CA1 **(E)** but it enhanced PPF in cortico-striatal fibers **(F)** after a delay of 100 or 150ms between pulses. **(G and H)** I/O relationships were overall similar in response to HDACi and rotarod training in the Schaffer Collaterals of CA1 **(G)** or cortico-striatal fibers **(H)**. Graphs represent mean ±SEM. * $P < 0.05$, ** $P < 0.01$, ns = not significant. n (striatum) = 10 animals per rotarod task/treatment, 8 animals per no task/treatment; n (hippoampus) = 6 animals/group.

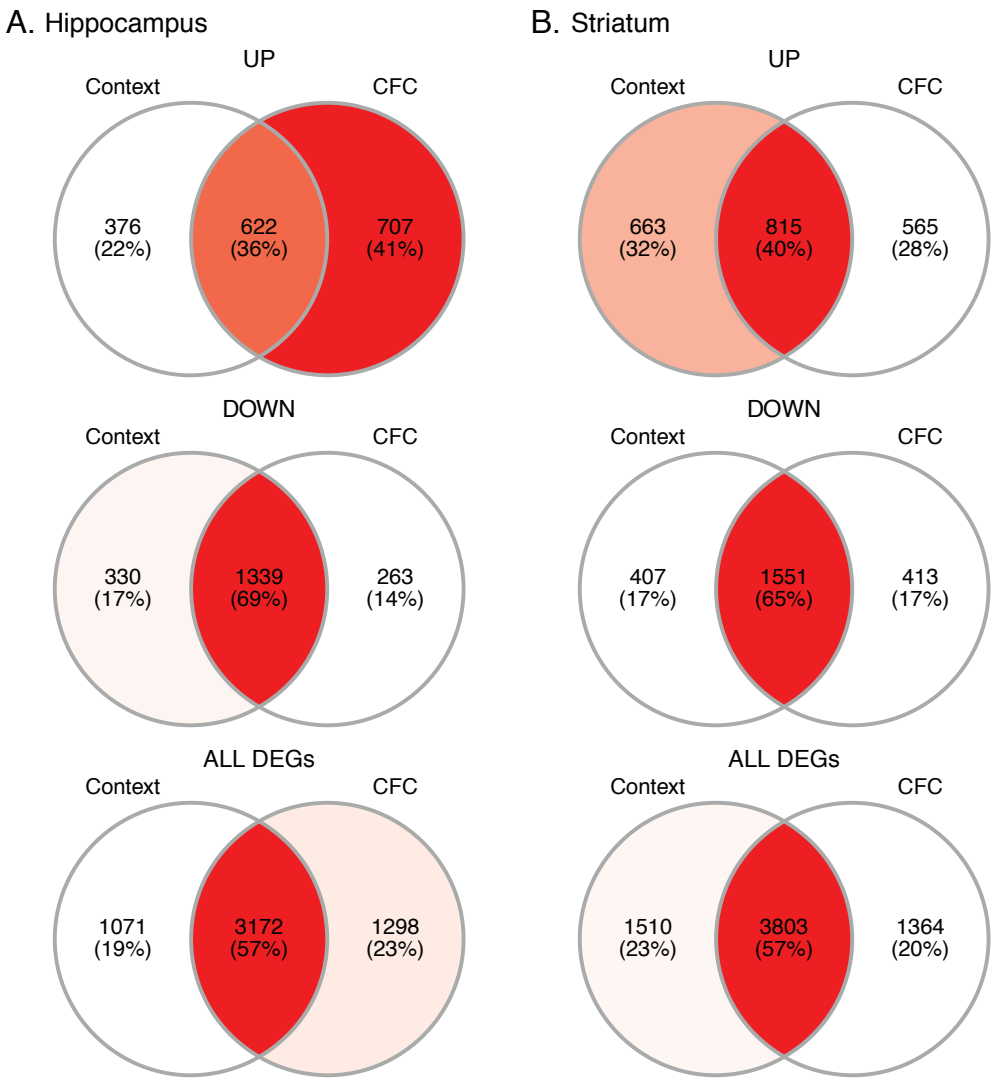

Supplemental Fig. 5. Overlap of differentially expressed genes (DEGs) by HDACi paired with context or CFC. Venn diagrams of genes that are upregulated (top), downregulated (middle row) or differentially expressed in either direction (bottom) in the context pair-wise comparison (HDACi-Context vs VEH-Context) and the CFC pair-wise comparison (HDACi-CFC vs VEH – CFC) in the hippocampus **(A)** and the striatum **(B)**.

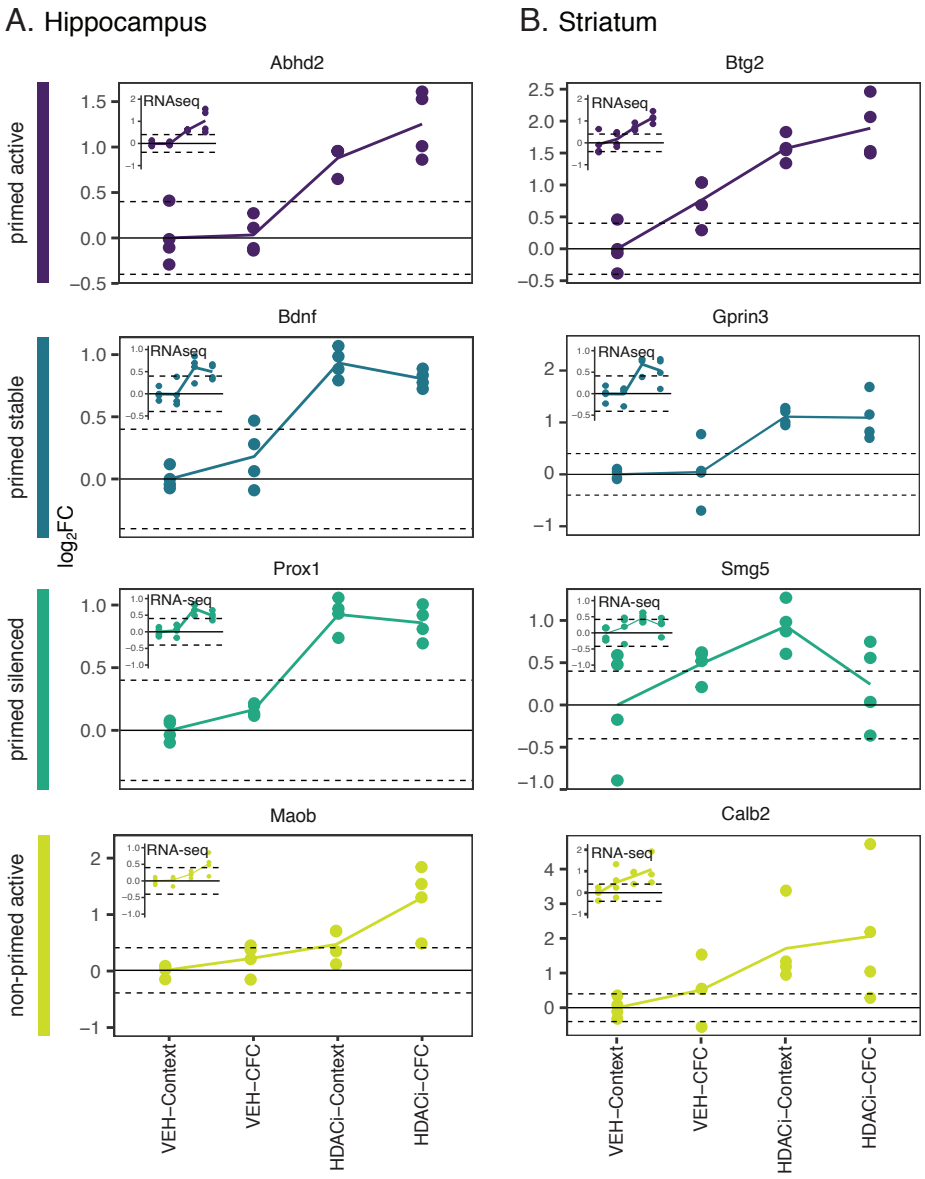

Supplemental Fig. 6. Validation of the bulk RNA-seq analysis by qRT-PCR. Example qRT-PCR fold change expression of genes in each trajectory for the hippocampus **(A)** and striatum **(B)**. Insets represent log_2FC comparisons of these genes from the RNA-seq analysis. Points represent calculated log_2FC for each biological replicate compared to the average VEH-Context. Lines represent the average log_2FC for each group. n = 4 animals/group.

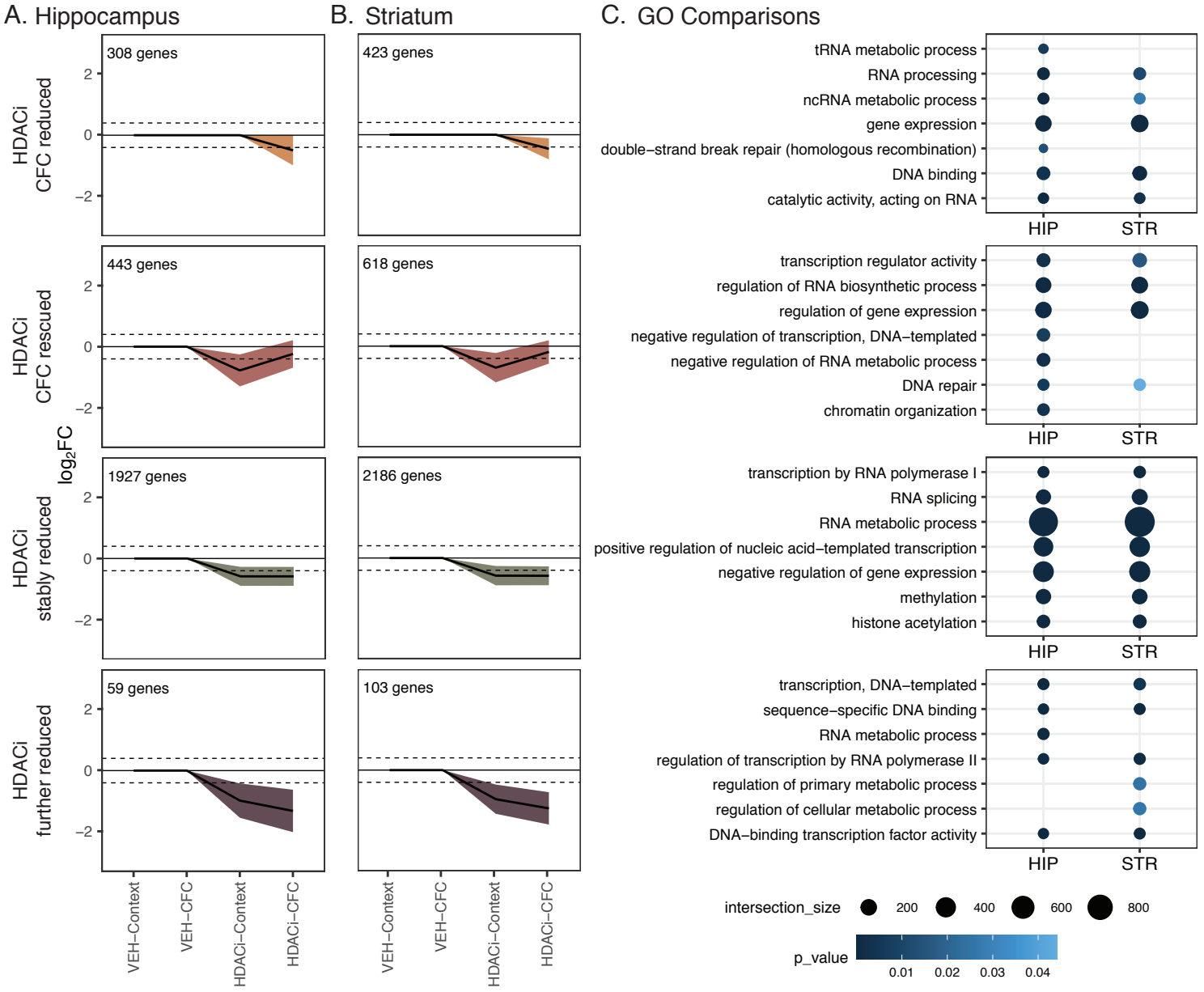

Supplemental Fig. 7. Clusters representing downregulated genes in the hippocampus and the striatum. Both the hippocampus **(A)** and striatum **(B)** included similar numbers of genes that were downregulated after combining HDACi with CFC ("HDACi CFC reduced", top) and genes that were reduced by HDACi-Context treatment but rescued by HDACi-CFC ("HDACi CFC rescued", second from top). Both brain regions also included genes that were stably reduced by HDACi treatment, regardless of the behavioral paradigm ("HDACi stably reduced", third from top) and genes that were reduced by HDACi-Context and further reduced by HDACi-CFC ("HDACi further reduced", bottom). **(C)** Examples of gene ontologies (GOs) from the hippocampus (left) and striatum (right) for the trajectory in the corresponding row. Line plots represent mean ±SEM.

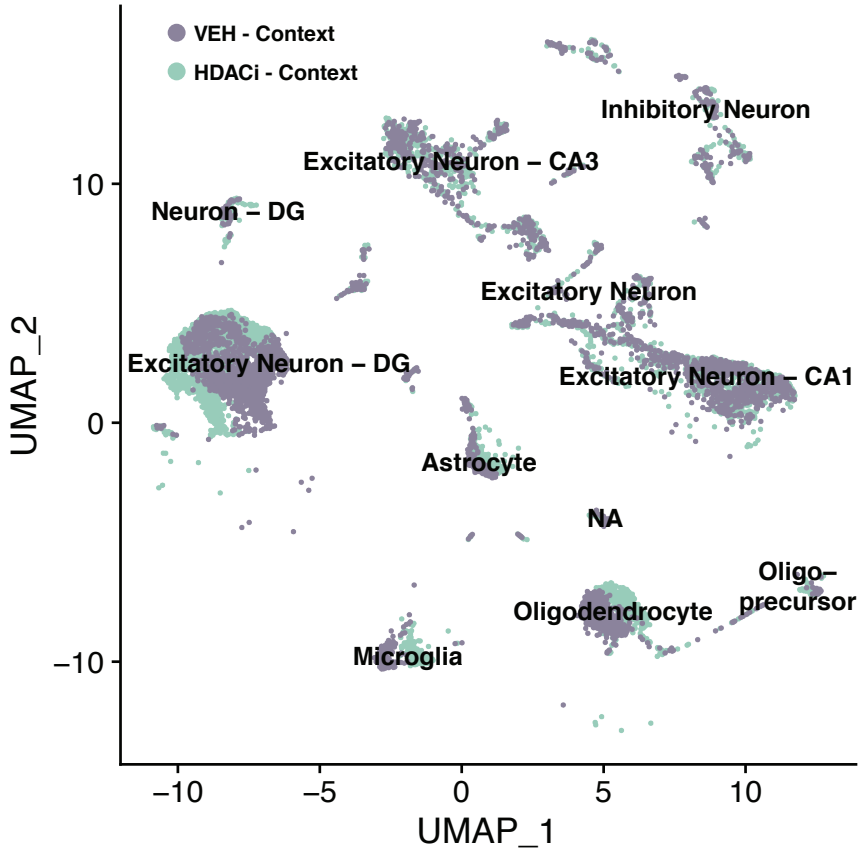

Supplemental Fig. 8. UMAP projection of samples taken after context only exposure (Context). Note that although the same cell types are represented in the CFC (Fig. 3D) and Context comparisons, there is no HDACi-mediated split in the Excitatory Neurons of the DG. Only glial clusters split after HDACi treatment paired with context exposure.

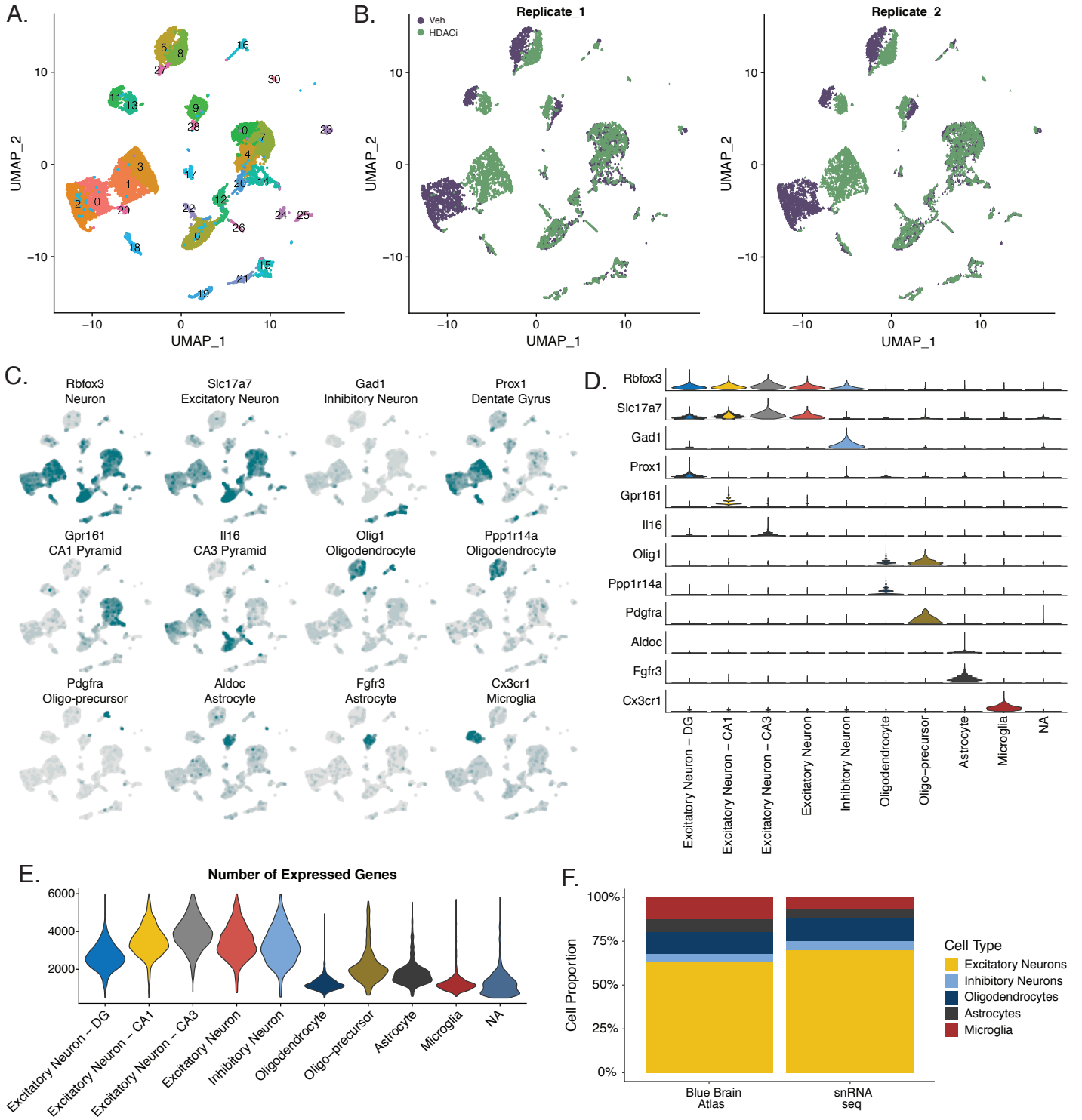

Supplemental Fig. 9. snRNA-Seq cell type assignments. (A) snRNA-seq gene count matrices were merged, filtered and normalized using SCTransform and underwent UMAP clustering. **(B)** UMAP projection of drug treatment replicates. **(C)** Clusters were assigned to cell types by overlaying UMI expression for known cell type markers over each cluster. **(D)** Clusters were assigned to cell types and hippocampal regions based on cell type markers with the highest UMI expression in each cluster. **(E)** Nuclei assigned to neuronal cell types had more expressed genes than glial cell types (oligodendrocytes, oligo-precursors, astrocytes and microglia). **(F)** Cell type assignments (right column) were similar to known cell proportions in the hippocampus, taken from the Blue Brain Atlas (left column), irrespective of drug and behavioral treatment. n = 2 biological replicates/group (HDACi-CFC and VEH-CFC).

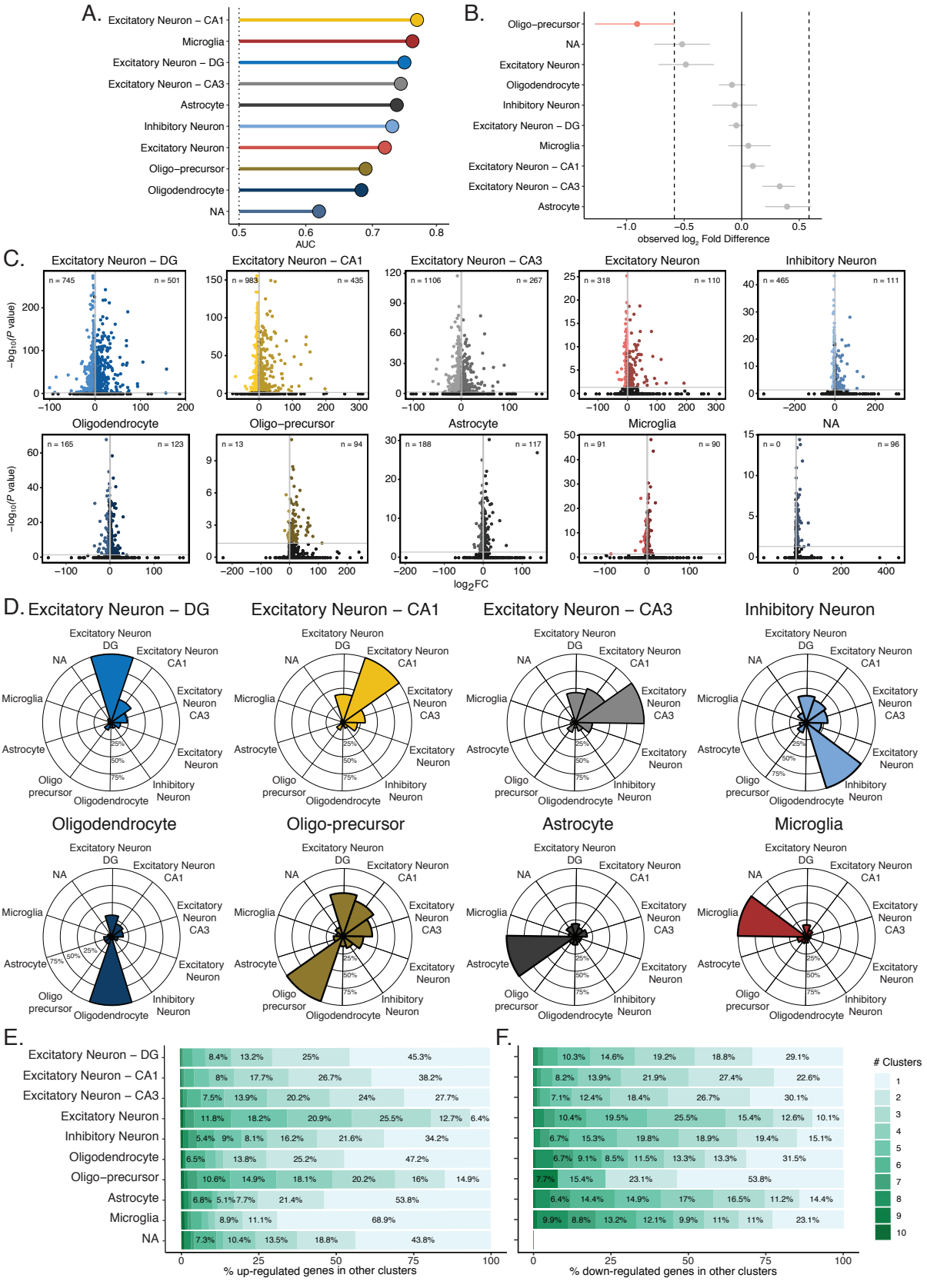

Supplemental Fig. 10. HDACi perturbs distinct gene sets in different cell types. (A) Augur analysis. Area under the receiver operating characteristic curve (AUC) is above random chance (0.5) for all cell types. **(B)** Cell type composition permutation test (#permutations = 1000). **(C)** Volcano plots showing magnitude of differential expression ($log_2FC \geq 1$; adjusted p-value ≤ 0.05) versus statistical significance ($-log_{10}$ P-value) for HDACi-CFC compared to VEH-CFC in each cell type. **(D)** Overlap of upregulated genes across cell types. **(E and F)** Percent of genes found in other clusters for each cell type. Genes that were found in only one cluster are unique to that cell type for upregulated **(E)** and downregulated **(F)** genes in each cluster.

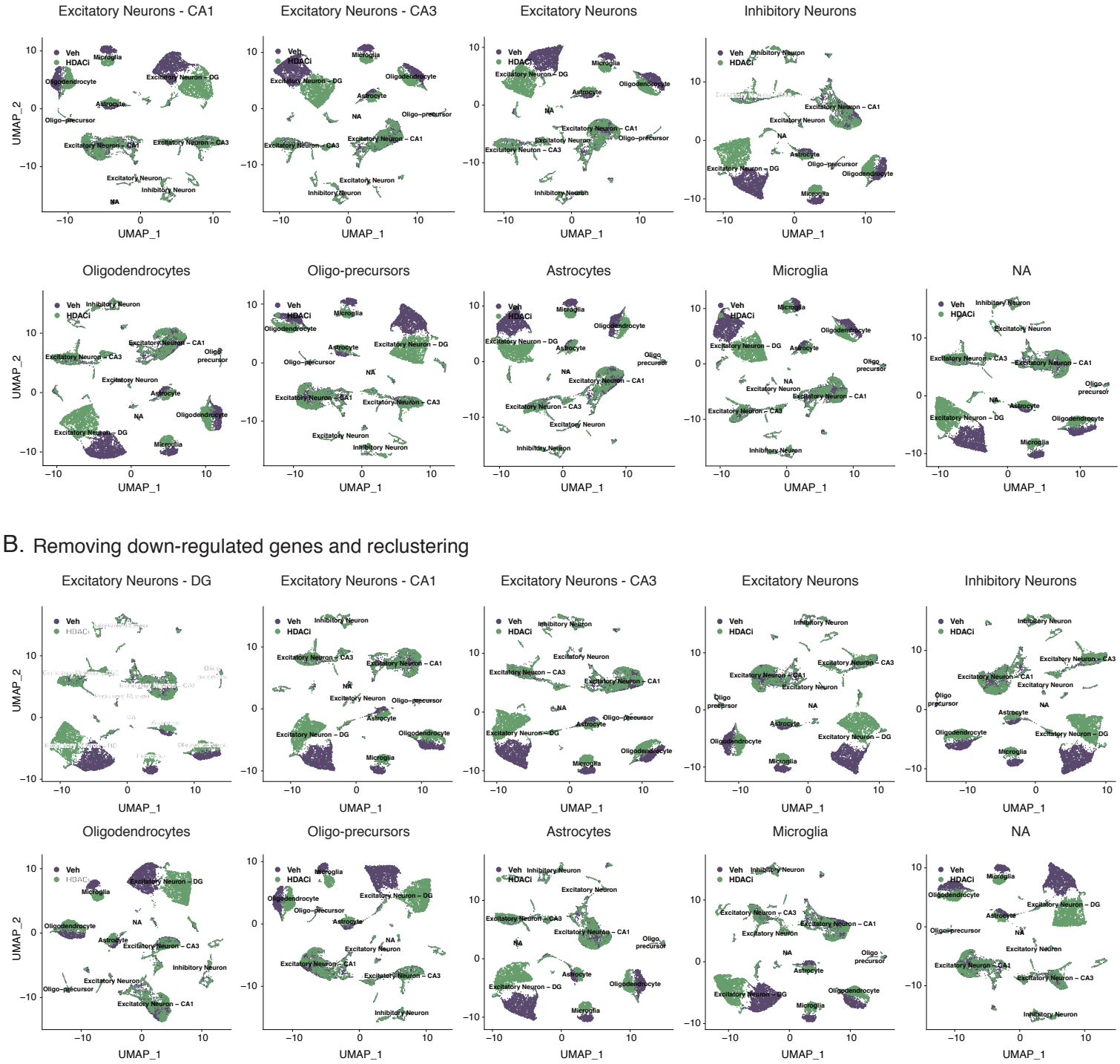

Supplemental Fig. 11. Removing up- and downregulated genes and re-running UMAP to determine unique gene sets. Removing up **(A)** and downregulated **(B)** genes and re-running UMAP clustering revealed whether the HDACi-induced differential expression calculated for each cell type was unique for that cell type. For example, removing upregulated genes from astrocytes remerged the astrocyte cluster in the UMAP, whereas removing downregulated genes did not.

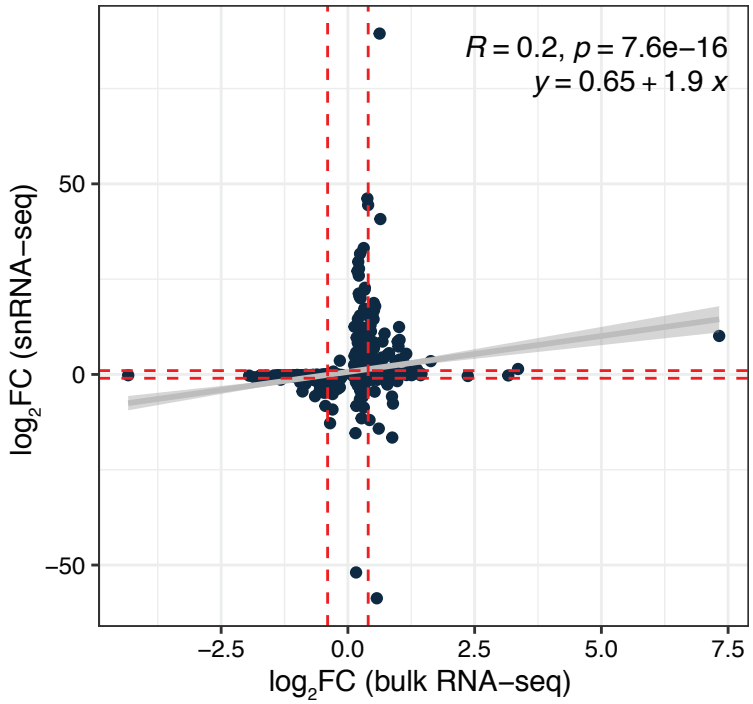

Supplemental Fig. 12. Log_2FC comparison of genes that are significant (p-value ≤ 0.05) in both bulk and snRNAseq analyses. Of the 7601 genes that were expressed in both the bulk and snRNA-seq (Excitatory Neurons of the DG), 1517 had a significant log_2FC in the HDACi-CFC vs. VEH-CFC comparisons. Most of these genes were differentially expressed in the same direction as 251 genes were upregulated ($log_2FC > 0$) and 1126 were downregulated ($log_2FC < 0$) in both experiments, which is illustrated by the significant correlation between the two types of analyses. In addition, there are 135 genes that were upregulated in the bulk comparison, but downregulated in the snRNA comparison, and there are 5 genes that were upregulated in the snRNA comparison, but downregulated in the bulk comparison.

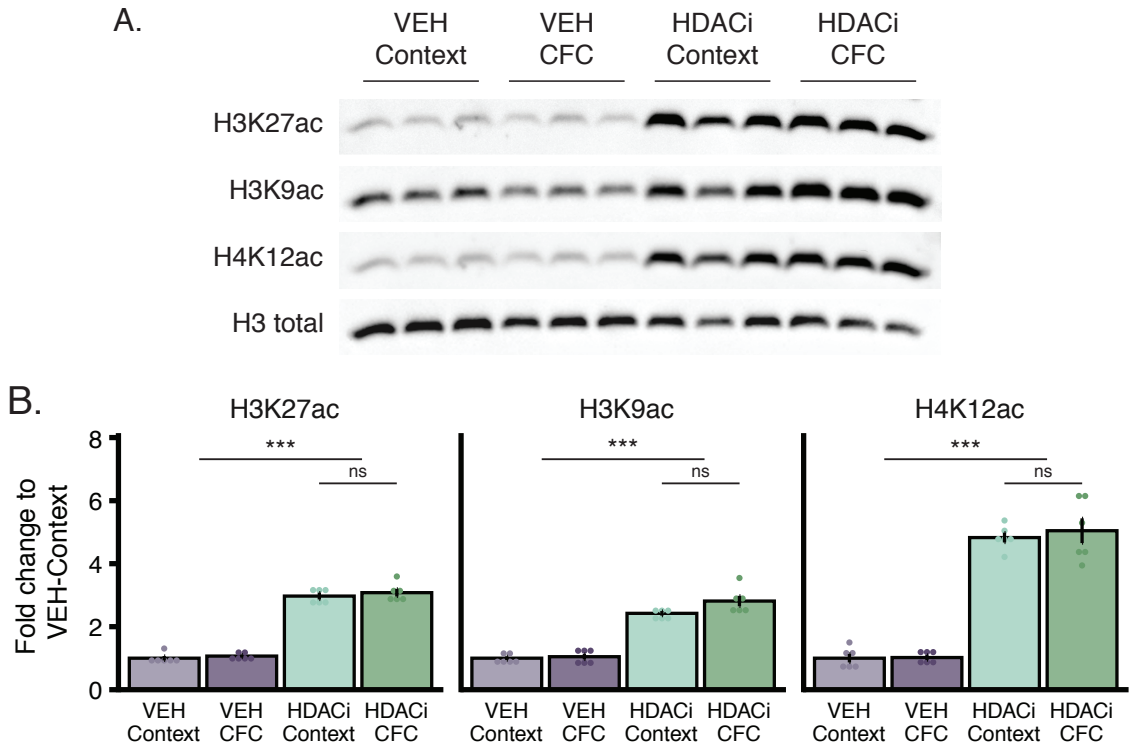

Supplemental Fig. 13. HDACi enriches H3K27, H3K9 and H4K12 acetylation regardless of behavioral condition. (A) Representative Western blot for hippocampal H3K27ac, H3K9ac and H4K27ac for all four treatments compared to total H3 abundance. **(B)** Western blot quantification for H3K27ac, H3K9ac and H4K12ac plotted as fold change to the average VEH-Context luminescence. Graphs represent mean ±SEM. n = 6 biological replicates per group, each with 2 technical replicates. Two-way ANOVA, *** $P < 0.001$, ns = not significant.

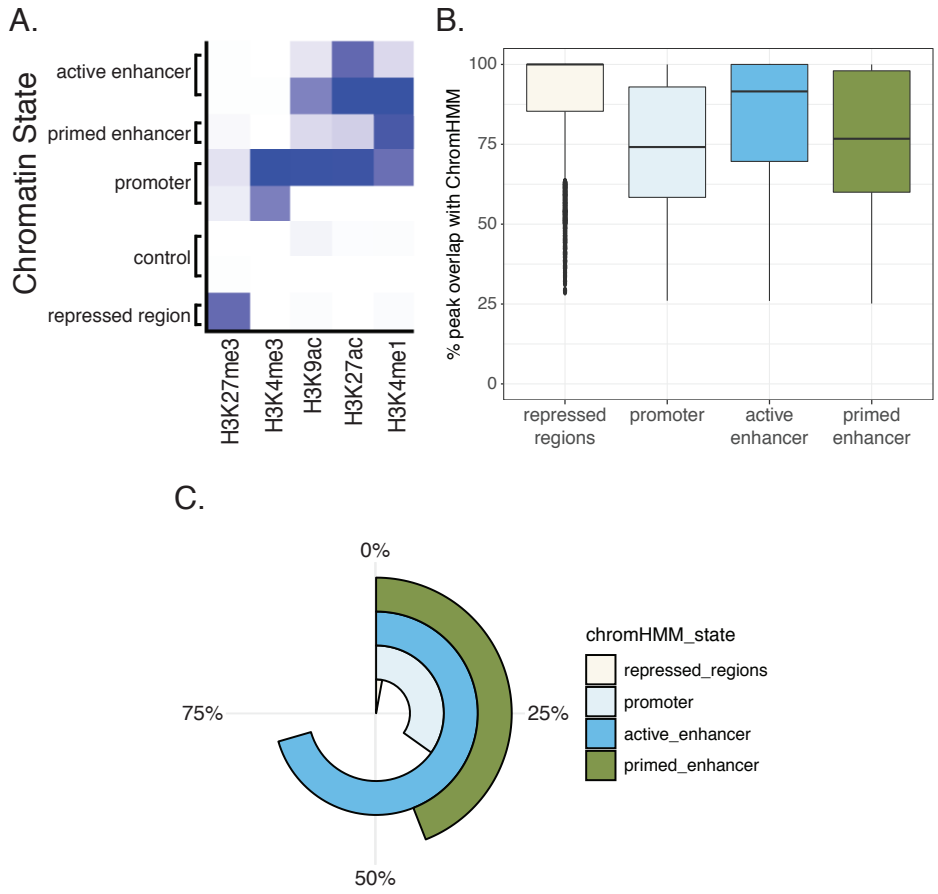

Supplemental Fig. 14. H3K27ac peaks at enhancer and promoter regions. (A) Five distinct chromatin states were assigned to the full mm10 genome using previously published histone PTMs and ChromHMM. H3K27me3 acts as a repressive marker, H3K4me3 and H3K9ac are promoter markers, H3K27ac is a marker of active enhancers and H3K4me1 is enriched at primed enhancers. **(B)** Percent of peak overlap with assigned chromatin states shows that most peaks overlap with their assigned state by more than 50%. Graphs shown as box and whisker plots with outliers plotted as points. **(C)** Proportion of each chromatin state enriched by H3K27ac peaks in all four treatments indicates that H3K27ac peaks are enriched at active and primed enhancers and not repressed regions.

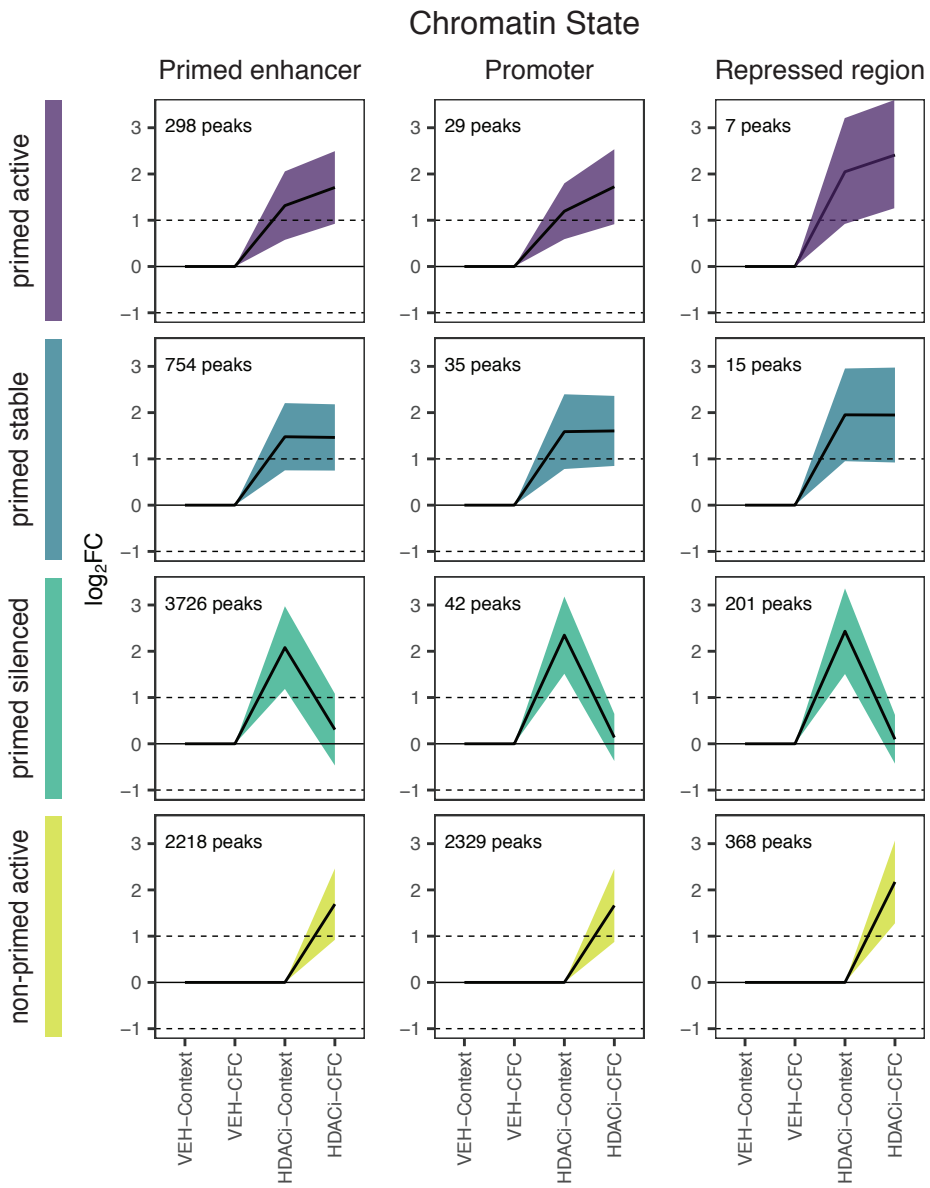

Supplemental Fig. 15. Trajectory analysis for H3K27ac peaks not associated with active enhancers. Line graphs in trajectory plots represent significant log_2FC values for each group in clusters of interest for primed enhancers (left), promoters (middle) and repressed regions (right). Count in upper left corner indicates the number of genes in each cluster. Line plots shown as mean ±SEM.

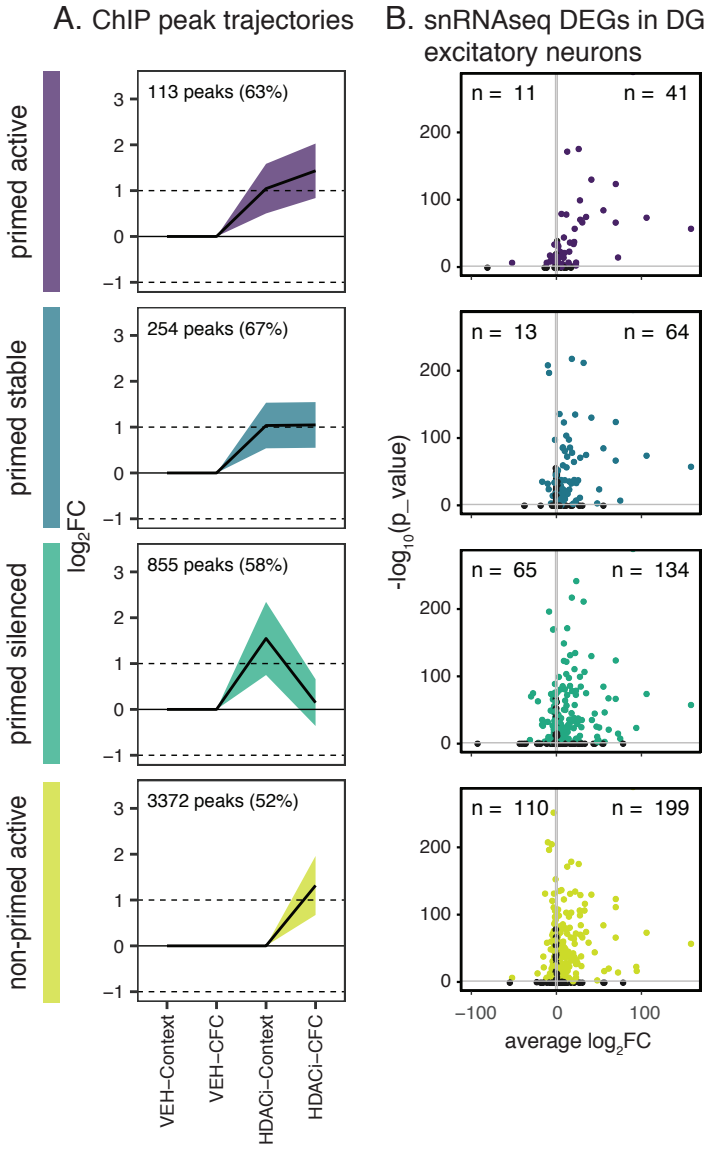

Supplemental Fig. 16. Genes associated with active enhancers in the ChIP-seq trajectory analysis that are differentially expressed in excitatory neurons of the DG. (A) Trajectory plots representing changes in H3K27ac in active enhancers that are also expressed in the excitatory neurons of the DG in the snRNA-seq. Values in upper left corners indicate numbers of overlapping genes and percent of genes from each trajectory in Fig 4D. Line plots shown as mean ±SEM. **(B)** Volcano plots for genes that are expressed in the excitatory neurons of the DG and are present in the respective trajectory of interest in the ChIP-seq analysis. Most genes that have increased H3K27ac at active enhancers are also up regulated in the excitatory neurons of the DG. n-values in corners represent the genes that are up regulated ($log_2FC \geq 1$; adjusted *P*-value ≤ 0.05).